

# Accelerated Computational Analysis of Metal–Organic Frameworks for Oxidation Catalysis

Konstantinos D. Vogiatzis,<sup>†,‡</sup> Emmanuel Haldoupis,<sup>†</sup> Dianne J. Xiao,<sup>‡</sup> Jeffrey R. Long,<sup>\*,‡,§</sup>  
J. Ilja Siepmann,<sup>\*,†,||</sup> and Laura Gagliardi<sup>\*,†</sup>

<sup>†</sup>Department of Chemistry, Minnesota Supercomputing Institute, and Chemical Theory Center, University of Minnesota, 207 Pleasant Street Southeast, Minneapolis, Minnesota 55455-0431, United States

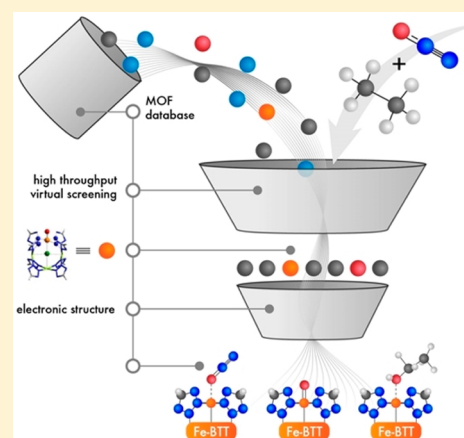
<sup>‡</sup>Department of Chemistry, University of California, Berkeley, California 94720, United States

<sup>§</sup>Materials Sciences Division, Lawrence Berkeley Laboratory, Berkeley, California 94720, United States

<sup>||</sup>Department of Chemical Engineering and Materials Science, University of Minnesota, 421 Washington Avenue SE, Minneapolis, Minnesota 55455-0431, United States

## Supporting Information

**ABSTRACT:** High-spin iron(IV)–oxo compounds are known to activate strong C–H bonds. Stabilizing the high-spin  $S = 2$  electronic configuration is difficult in molecular species for homogeneous catalysis, but recent experimental and computational results suggest this can be achieved in the metal–organic framework  $\text{Fe}_2(\text{dobdc})$  ( $\text{dobdc}^{4-} = 2,5\text{-dioxido-1,4-benzenedicarboxylate}$ ) and its magnesium-diluted analogues. With a novel computational screening approach, we have identified three additional frameworks that are predicted to form high-spin iron(IV)–oxo species upon dissociative adsorption of nitrous oxide. The computational work is supported by follow-up experiments which show that, among these three materials, Fe-BTT (BTT<sup>3-</sup> = 1,3,5-benzenetris-tetrazolate) selectively oxidizes ethane to ethanol at 120 °C. Subsequent spectroscopic and cycling studies suggest that framework defects, rather than the bulk framework or extraframework sites, are likely responsible for the observed reactivity. This work shows how computational methods can be used to rapidly identify promising candidate frameworks, and highlights the need for new methods that allow defect sites in metal–organic frameworks to be better understood and exploited for catalysis.



## INTRODUCTION

High-valent iron(IV)–oxo species of heme and non-heme iron enzymes have been invoked as key reactive intermediates in important metabolic transformations.<sup>1</sup> The synthesis and characterization of non-heme iron(IV)–oxo model complexes has enabled the understanding of the physical and chemical properties of their enzymatic analogue intermediates.<sup>2–5</sup> These biomimetic catalysts are typically formed upon reaction with oxo transfer reagents, such as hydrogen peroxide, iodossylbenzene, or dioxygen, and can activate the strong C–H bonds of alkanes. Mechanistic and theoretical studies in a variety of synthetic model complexes have underlined the role of the iron spin state in the catalytic activity of this reactive intermediate.<sup>2–5</sup> In particular, it has been recognized that the high-spin  $S = 2$  iron(IV)–oxo unit of non-heme complexes is the more reactive species<sup>6–8</sup> and favors the H-abstraction reaction. However, the first synthetic non-heme  $S = 2$  iron(IV)–oxo complexes<sup>9–11</sup> exhibited reactivity similar to  $S = 1$  systems, likely due to steric protection of the oxo unit by bulky ligand substituents.<sup>12</sup>

Apart from enzymes and synthetic molecular complexes, porous solid materials have been suggested as alternative hosts of high-valent iron–oxo intermediates. Catalytic sites can be created either as part of the framework or as deposited single-iron cations. For example, the zeolite Fe–ZSM-5 (ZSM = zeolite Socony Mobil) can oxidize methane to methanol after pretreatment with  $\text{N}_2\text{O}$ ,<sup>13</sup> though the reaction mechanism is not well understood. Recently, the magnesium-diluted  $\text{Fe}_{0.1}\text{Mg}_{1.9}(\text{dobdc})$  metal–organic framework ( $\text{dobdc}^{4-} = 2,5\text{-dioxido-1,4-benzenedicarboxylate}$ ) was shown to oxidize ethane to ethanol in the presence of nitrous oxide, with theoretical calculations suggesting an  $S = 2$  iron(IV)–oxo intermediate.<sup>14,15</sup> The high-spin state is preferred due to the weak-field carboxylate and aryl oxide ligand environment.

Compared to molecular chemistry, where a tripodal ligand has been successfully used in the synthesis of high-spin non-heme model complexes,<sup>9–11</sup> the coordination environment of the metal sites within a metal–organic framework can be

Received: July 15, 2016

Published: July 28, 2016

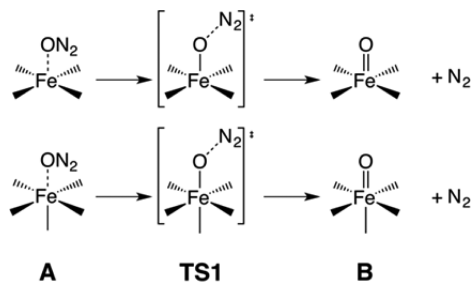
substantially different, as in the case of the  $M_2(\text{dobdc})$  family of materials. The  $\text{dobdc}^{4-}$  linker possesses carboxylate and aryl oxide functional groups. Those form a weak ligand field around the metal center and, like the nitrogen-based chelating tripodal ligands of non-heme model complexes, support the stabilization of a high-spin  $S = 2$  iron(IV)–oxo intermediate. In synthetic materials with weak ligand fields, the quintet channel may be significantly lower than the triplet channel, avoiding the two-state reactivity scheme<sup>16</sup> and spin inversions during the reaction. This hypothesis was recently verified in a synthetic non-heme iron(IV)–oxo model complex that exhibits a weaker octahedral ligand environment with a remarkably higher reactivity.<sup>17</sup>

In principle, other iron-based metal–organic frameworks with similar weak-field coordination environments should also support this type of chemistry.<sup>5,18</sup> While thousands of metal–organic frameworks have been reported in the literature, identifying, synthesizing, and experimentally testing each potential candidate is laborious and impractical. To accelerate this process, we developed a novel algorithm to computationally screen large databases of known metal–organic frameworks for structures containing coordinatively unsaturated metal sites. In particular, the focus of this work is the detection of a coordinatively unsaturated iron(II) center within a stable porous framework that can activate  $\text{N}_2\text{O}$  and support a high-spin iron(IV)–oxo intermediate. Combination of the screening algorithm with electronic structure calculations identified three already-synthesized metal–organic frameworks that can activate  $\text{N}_2\text{O}$ . Experimental work verified the computational results by demonstrating that one of these materials can oxidize ethane to ethanol in the presence of  $\text{N}_2\text{O}$ , but also highlighted the role of defect sites in metal–organic framework catalysis.

## RESULTS AND DISCUSSION

The steps for the oxidation of ethane to ethanol in the presence of  $\text{N}_2\text{O}$  within the pores of  $\text{Fe}_{0.1}\text{Mg}_{1.9}(\text{dobdc})$  have already been identified computationally,<sup>15,19</sup> and were used as reference in our analysis. The first step of this reaction is the adsorption of  $\text{N}_2\text{O}$  in the vacant position of the pentacoordinated iron(II) center to form intermediate **A** (Scheme 1). The terminal

**Scheme 1. Drawing of Intermediates A and B, and the Transition State (TS1) for Tetra- (top) and Pentacoordinated (bottom) Molecular Clusters**



oxygen is transferred from  $\text{N}_2\text{O}$  to the iron center to form the iron(IV)–oxo intermediate **B**. The rate-determining step of this process corresponds to the cleavage of the N–O bond of  $\text{N}_2\text{O}$  and the release of dinitrogen via the first transition state **TS1** (Scheme 1). A barrier of 82 kJ/mol was obtained previously for **TS1** in  $\text{Fe}_{0.1}\text{Mg}_{1.9}(\text{dobdc})$ .<sup>15</sup>

Our computational screening algorithm was applied to a database of over 5000 known metal–organic frameworks. The procedure to detect open metal sites in metal–organic frameworks is based on an analysis of the reported crystallographic coordinates. First, we identify all the structures in the computation-ready experimental (CoRE) metal–organic framework database<sup>20</sup> that contain Fe atoms. Second, for each Fe atom, the coordination sphere consisting of all atoms directly bound to the Fe atom is analyzed. Geometric criteria, based on the bond and torsion angles between the central Fe atom and the atoms in the coordination sphere, are used to distinguish whether a Fe atom can be considered as open or not.<sup>21</sup> Third, the pore structure is analyzed to assess whether the undercoordinated Fe atom is accessible to guest molecules.

Application of our computational screening tool on the CoRE metal–organic framework database identified 46 metal–organic frameworks with undercoordinated Fe centers out of 150 Fe-containing metal–organic frameworks. Some of these structures were discarded prior to any further computational analysis based on specific considerations, such as the instability of the framework upon removal of the solvent, the inaccessibility of the open site, the oxidation state of iron, or being isostructural to  $\text{Fe}_2(\text{dobdc})$ . This nonautomated process reduced the number of metal–organic framework candidates from 46 to 7. The Cambridge Crystallographic Structure Database reference codes of the seven selected materials are YUCZOM (1),<sup>22</sup> ISUCUV (2),<sup>23</sup> DAXHIV (3),<sup>24</sup> XESKUD (4),<sup>25</sup> MUWQEB (5),<sup>26</sup> FUFREE (6),<sup>27</sup> and RULXOM (7).<sup>28</sup>

The formation and stability of the high-spin iron(IV)–oxo intermediate in these seven frameworks (1–7, Figure 1) were examined by density functional theory (DFT) calculations. A two-step procedure was applied to assess the formation of the high-spin iron(IV)–oxo species (intermediate **B**): first, the relative electronic energy differences between the high-, intermediate-, and low-spin states ( $S = 2, 1,$  and  $0,$  respectively) of **B** for each of the seven model complexes were calculated; second, the energy barrier associated with **TS1** was computed.

The DFT calculations support our hypothesis that metal–organic frameworks featuring weak-field ligands offer a preferential coordination environment for the highly reactive  $S = 2$  (quintet) iron(IV)–oxo intermediate. Five (1–5) of the seven single-iron models exhibit a large quintet–triplet energy gap which clearly favors the  $S = 2$  spin state (see Table 1). In particular, an energy gap comparable to that of  $\text{Fe}_{0.1}\text{Mg}_{1.9}(\text{dobdc})$  (8, Figure 1) is found for **1**, in which the carboxylic and pyridine-type organic linkers create a weak ligand field around the iron center that stabilizes the high-spin state. In contrast, two competitive reactive channels are expected for **6** and **7** (high and intermediate spin).

While previous preparations of reactive iron–oxo intermediates in porous materials have successfully utilized the gaseous oxidant  $\text{N}_2\text{O}$ , it is kinetically inert and its decomposition is often the rate-limiting step.<sup>13,14</sup> Therefore, we subsequently calculated reaction barriers of the N–O bond cleavage on the iron centers for the seven candidate materials. For three cases (1, 4, and 6), the calculations predict that there is no  $\text{N}_2\text{O}$  binding on the open Fe site. Unconstrained geometry optimizations yield weak binding of  $\text{N}_2\text{O}$ , but with significantly distorted structures, indicating a high degree of instability for these frameworks. Contrastingly, favorable  $\text{N}_2\text{O}$  binding was found for four out of the seven candidate materials (2, 3, 5, and 7), with three of them (2, 3, and 5) having a comparable barrier to the reference material **8** (Table 1).

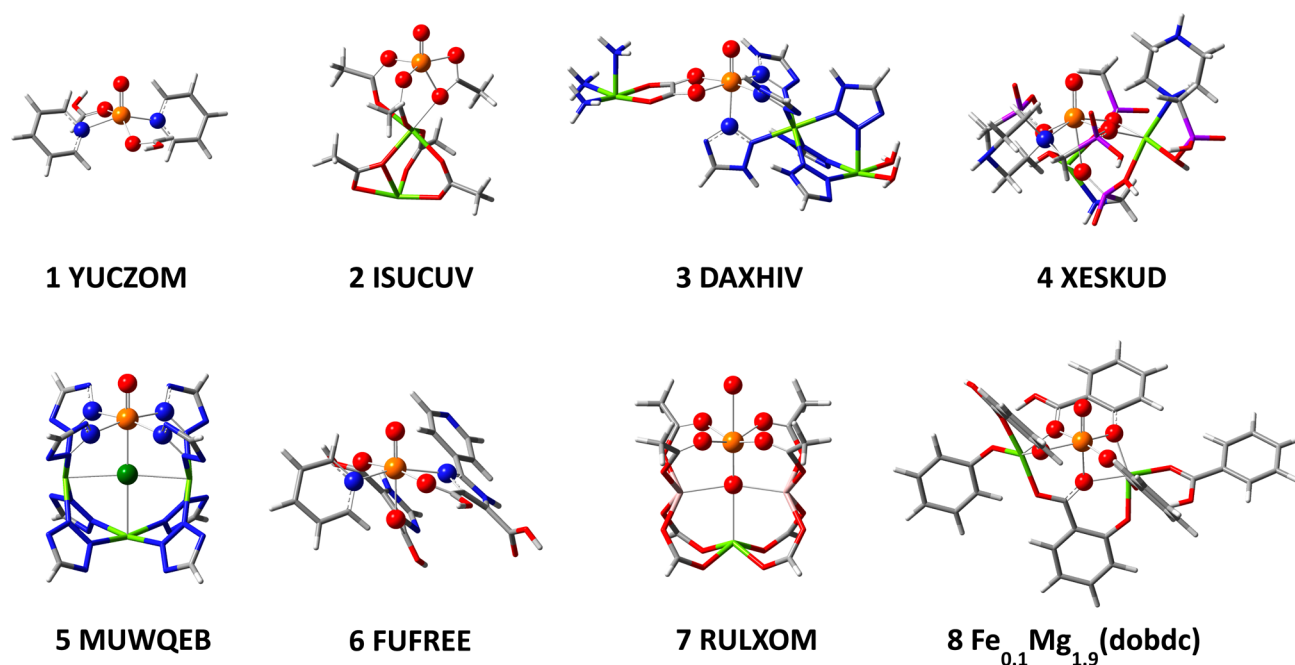


**Figure 1.** Optimized structures of the iron(IV)–oxo intermediate for the seven metal–organic frameworks investigated in detail in this study. Structure 8 corresponds to the iron(IV)–oxo intermediate of the  $\text{Fe}_{0.1}\text{Mg}_{1.9}(\text{dobdc})$  reference material. Color code: orange = Fe, light green = Mg, pink = Al, dark green = Cl, purple = P, blue = N, red = O, gray = C, white = H.

**Table 1. Relative Energy Differences between Intermediate- and High-Spin States ( $\Delta E_{\text{IS-HS}}$ ) and Reaction Enthalpy Barriers ( $\Delta E_{\text{TS1-A}}$ ) of the Seven Cluster Models<sup>a</sup>**

	1	2	3	4	5	6	7	8 <sup>b</sup>
$\Delta E_{\text{IS-HS}}$	131	93	86	85	66	1	0	136 <sup>c</sup>
$\Delta E_{\text{TS1-A}}$	–	77	88	–	65	–	280	82 <sup>d</sup>

<sup>a</sup>All values in kJ/mol. <sup>b</sup>Reference material. <sup>c</sup>From ref 14. <sup>d</sup>From ref 15.

To confirm these theoretical predictions, experimental studies were performed on two of the candidate frameworks: **5** and **7**. Compound **7**, also known as PCN-9(Fe) (PCN = porous coordination network), was predicted to show no  $\text{N}_2\text{O}$  reactivity. Compound **5**, also known as Fe-BTT ( $\text{BTT}^{3-} = 1,3,5\text{-benzenetrizotrazolate}$ ), was predicted to have a reactivity similar to that of  $\text{Fe}_{0.1}\text{Mg}_{1.9}(\text{dobdc})$ . In initial test reactions, both PCN-9(Fe) and Fe-BTT were treated with a 1:7 mixture of  $\text{N}_2\text{O}$  and ethane at 14 bar, and heated to 120 °C for 14 h. As theory suggested, no ethane oxidation was observed using PCN-9(Fe). On the other hand, under identical conditions Fe-BTT was found to oxidize ethane to ethanol with no observable overoxidation or side products, albeit in relatively low yields (0.04 equiv per framework iron). After this treatment, Fe-BTT retains its high crystallinity, as confirmed by powder X-ray diffraction (see [Supporting Information](#)). In addition, unlike  $\text{Fe}_{0.1}\text{Mg}_{1.9}(\text{dobdc})$ , where the iron sites have been shown to decay into inactive Fe(III) hydroxide or alkoxide species after prolonged  $\text{N}_2\text{O}$  exposure, Mössbauer studies showed that >90% of the iron centers in Fe-BTT remain in the +2 oxidation state after  $\text{N}_2\text{O}$ /ethane treatment (see [Supporting Information](#)).

Prompted by the modest conversions observed experimentally, subsequent efforts were undertaken to elucidate the active site responsible for ethane oxidation in Fe-BTT. Because the base framework for Fe-BTT is anionic, the material contains both framework cations (which were computationally inves-

tigated above) and charge-balancing extraframework iron(II) centers, in a ratio of 24:3. These extraframework cations have been located crystallographically in other M-BTT frameworks,<sup>29,30</sup> and typically reside between two neighboring tetrazolates. Thus, despite the deceptively high symmetry of its crystal structure, the iron(II) centers in Fe-BTT are not all spectroscopically identical. Indeed, the Mössbauer spectrum of DMF-solvated Fe-BTT reveals five different iron(II) environments (one extraframework and four framework sites).<sup>25</sup>

In order to rule out the involvement of extraframework sites, the extraframework  $\text{Fe}^{2+}$  cations were postsynthetically exchanged with  $\text{Zn}^{2+}$  cations. Treating Fe-BTT with excess  $\text{ZnCl}_2$  at room temperature in methanol<sup>31</sup> led to the formation of Zn/Fe-BTT, which contains 18% Zn as determined by ICP analysis. These ICP results indicate that all the extraframework and a small percentage of the framework cations (~7–8%) have been displaced. Zn/Fe-BTT can be desolvated by heating to 130 °C for 24 h, leading to a porous material with a Brunauer–Emmett–Teller (BET) surface area of 1835(7)  $\text{m}^2/\text{g}$  (Langmuir surface area = 1982(11)  $\text{m}^2/\text{g}$ ). The Mössbauer spectrum of the activated material reveals three slightly different iron(II) sites, which we assign as (a) framework Fe(II) centers in tetranuclear building units containing no Zn(II) (79%), (b) framework Fe(II) centers directly adjacent to a framework Zn(II) site (14%), and (c) framework Fe(II) centers directly across a Zn(II) site, linked by the  $\mu_4$ -chloride bridge (7%) (see [Supporting Information](#)).

Treatment of activated Zn/Fe-BTT with  $\text{N}_2\text{O}$  and ethane, under the same conditions as Fe-BTT, also leads to exclusive ethanol formation (~0.04 equiv per framework iron site). Because these results are identical to the parent Fe-BTT framework, it is highly unlikely that the extraframework cations are responsible for the observed reactivity. Like Fe-BTT, Mössbauer studies show that the majority of the iron sites in Zn/Fe-BTT remain in the +2 oxidation following  $\text{N}_2\text{O}$ /ethane treatment, with only slight changes in the Mössbauer

parameters of the three iron sites (see Supporting Information). In addition, the posttreatment framework maintains both its crystallinity and surface area (see Supporting Information).

Next, we investigated whether the recycled framework is capable of oxidizing ethane. The recovered material was reactivated and reexposed to  $\text{N}_2\text{O}$ /ethane at 120 °C. To our surprise, no ethanol formation was observed, even though the bulk of the Fe(II) sites in the recovered framework, as probed by Mössbauer studies, powder X-ray diffraction, and surface area measurements, are essentially identical to the pristine material. Following these results, we conclude that a very small fraction of the iron(II) sites, which have yet to be detected spectroscopically, are responsible for the initial reactivity but decay over the course of the first  $\text{N}_2\text{O}$ /ethane treatment. These sites could be the result of missing linkers, structural distortions due to thermal activation, surface sites, or crystal fractures, which have been previously shown to be important in metal–organic framework based catalysis.<sup>32–37</sup>

Why are the bulk framework sites inactive, even though computations suggest otherwise? An important factor may be the poor thermal stability of M-BTT frameworks. A fully desolvated Fe-BTT framework, which is what was investigated computationally, cannot be achieved in practice as the material is not stable above 135 °C. All the Fe-BTT derivatives studied experimentally contain roughly 30% solvent per framework cation. In addition, due to this thermal instability, a small amount of defects may arise during the activation process. Nodal transitions can occur at high temperatures without damage of the global framework.<sup>38</sup> Finally, M-BTT and related sodalite-type frameworks possess a relatively large degree of structural flexibility, with unit cells that can contract and expand significantly.<sup>39,40</sup>

While the true active site structure in Fe-BTT is still unknown, the weak-field tetrazolate environment undoubtedly plays an important role. Two related materials, Fe-BTTri ( $\text{H}_3\text{BTTri} = 1,3,5\text{-tri}(1H\text{-}1,2,3\text{-triazol-}5\text{-yl})\text{benzene}$ ) and Fe-BTP ( $\text{H}_3\text{BTP} = 1,3,5\text{-tri}(1H\text{-pyrazol-}4\text{-yl})\text{benzene}$ ), were also studied, and both show poorer reactivity profiles than Fe-BTT.<sup>40</sup> These materials possess the same overall structure as Fe-BTT, except the bridging tetrazolates are replaced with more electron-donating triazolate and pyrazolate moieties, respectively. Note that Fe-BTP is a new framework, which can be synthesized by heating  $\text{Fe}(\text{CF}_3\text{SO}_3)_2$ ,  $\text{H}_3\text{BTP}$ ,  $\text{NH}_4\text{Cl}$ , and dimethylformamidium trifluoromethanesulfonate in a mixture of methanol and dimethylformamide at 393 K (see Supporting Information). Due to the lower Lewis acidity of its framework cations, Fe-BTTri exhibits a less favorable isosteric heat of  $\text{N}_2\text{O}$  adsorption of  $-26 \pm 1$  kJ/mol which suggests very little  $\text{N}_2\text{O}$  binds to the open metal sites under the reaction temperatures (120 °C). For comparison, the DFT-calculated  $\text{N}_2\text{O}$  binding energy of  $\text{Fe}_2(\text{dobdc})$  is  $-45$  kJ/mol,<sup>14</sup> and the measured  $\text{N}_2\text{O}$  binding energy of Fe-BTT is slightly higher at  $-56(1)$  kJ/mol. In addition, Fe-BTTri shows ethane conversions similar to Fe-BTT (0.03 equiv of product per framework iron), but with small amounts of ether side products, while Fe-BTP, which utilizes a much more basic pyrazolate, shows no reactivity under these conditions.

## CONCLUDING REMARKS

Successful high-throughput screening studies involving large numbers of hypothetical or experimental porous structures have mainly focused on potential applications in gas storage and separations.<sup>41</sup> For other applications, such as catalysis or spin-

crossover phenomena, there is still much to be learned from already synthesized metal–organic frameworks. A theoretical, fundamental understanding of the structural and electronic properties of these known materials will help in designing and developing the next generation of functional frameworks. The present work moves the field of catalytic applications in metal–organic frameworks toward this direction. Our efforts to mimic nature's reactive intermediates of enzymes, such as the iron(IV)–oxo species, led us to identify seven Fe-containing frameworks from a database of more than 5000 established materials as candidates for catalyzing critical hydrocarbon oxidation reactions. Two criteria were applied for the further screening of the seven materials. The first, the N–O dissociation barrier of  $\text{N}_2\text{O}$ , suggests if the iron(IV)–oxo reactive intermediate can be formed. The second criterion, which is the energy difference between the  $S = 2$  and  $S = 1$  spin states of the iron(IV)–oxo intermediate, provides an estimate about the relative stability of the preferential, high-spin state. Electronic structure theory calculations suggested that three of the seven candidate frameworks can form the reactive iron(IV)–oxo intermediate, while the remaining four materials should be inactive. The previously reported mechanism of the oxidation of ethane to ethanol inside the pores of the  $\text{Fe}_{0.1}\text{Mg}_{1.9}(\text{dobdc})$  metal–organic framework was used as reference material.

Synergistic experimental and computational examination of two out of seven candidate materials showed that coordinatively unsaturated Fe(II) sites in a weak-field ligand environment can perform the oxidation of small alkanes. The compound Fe-BTT was computationally discovered and experimentally demonstrated to catalytically and selectively oxidize ethane to ethanol in the presence of  $\text{N}_2\text{O}$ . Unexpectedly, spectroscopic and cycling studies on cation-exchanged Fe-BTT suggest defects are largely responsible for the observed reactivity, highlighting how much still needs to be understood concerning defect sites in metal–organic frameworks. Future computational and experimental studies are needed to identify the true active sites in Fe-BTT, and may lead to promising new directions for oxidation catalysis in iron-based metal–organic frameworks.

The high-throughput computational screening tool applied here is transferable to other databases of porous materials, such as databases with hypothetical or newly synthesized metal–organic frameworks. Its applicability can be expanded for the study of other catalytic reactions and gas adsorption applications. However, structural defects that deviate from the ideal frameworks should be considered in future screening studies.

## ASSOCIATED CONTENT

### Supporting Information

The Supporting Information is available free of charge on the ACS Publications website at DOI: 10.1021/acs.jpcc.6b07115.

Details of computational screening, DFT calculations and results, experimental procedures, and characterization data (PDF)

## AUTHOR INFORMATION

### Corresponding Authors

\*E-mail: jrlong@berkeley.edu.

\*E-mail: siepmann@umn.edu.

\*E-mail: gagliard@umn.edu.

## Present Address

<sup>†</sup>Department of Chemistry, University of Tennessee, Knoxville, Tennessee 37996, United States.

## Author Contributions

The manuscript was written through contributions of all authors.

## Notes

The authors declare no competing financial interest.

## ACKNOWLEDGMENTS

This research was carried out within the Nanoporous Materials Genome Center, which is supported by the Department of Energy, Office of Basic Energy Sciences, Division of Chemical Sciences, Geosciences, and Biosciences under Award DE-FG02-12ER16362. This research used resources of the Advanced Photon Source, a U.S. Department of Energy (DOE) Office of Science User Facility operated for the DOE Office of Science by Argonne National Laboratory under Contract No. DE-AC02-06CH11357. The authors acknowledge the Minnesota Supercomputing Institute at the University of Minnesota for providing resources that contributed to the research results reported within this paper. We thank Prachi Sharma (UMN) for useful discussion.

## REFERENCES

- (1) Nam, W. High-Valent Iron(IV)–Oxo Complexes of Heme and Non-Heme Ligands in Oxygenation Reactions. *Acc. Chem. Res.* **2007**, *40* (7), 522–531.
- (2) Solomon, E. I.; Light, K. M.; Liu, L. V.; Srncic, M.; Wong, S. D. Geometric and Electronic Structure Contributions to Function in Non-heme Iron Enzymes. *Acc. Chem. Res.* **2013**, *46* (11), 2725–2739.
- (3) Hohenberger, J.; Ray, K.; Meyer, K. The biology and chemistry of high-valent iron–oxo and iron–nitrido complexes. *Nat. Commun.* **2012**, *3*, 720.
- (4) Rohde, J.-U.; In, J.-H.; Lim, M. H.; Brennessel, W. W.; Bukowski, M. R.; Stubna, A.; Münck, E.; Nam, W.; Que, L., Jr. Crystallographic and Spectroscopic Characterization of a Nonheme Fe(IV)=O Complex. *Science* **2003**, *299* (5609), 1037–1039.
- (5) Ray, K.; Pfaff, F. F.; Wang, B.; Nam, W. Status of Reactive Non-Heme Metal–Oxygen Intermediates in Chemical and Enzymatic Reactions. *J. Am. Chem. Soc.* **2014**, *136* (40), 13942–13958.
- (6) Ye, S.; Neese, F. Nonheme oxo-iron(IV) intermediates form an oxyl radical upon approaching the C–H bond activation transition state. *Proc. Natl. Acad. Sci. U. S. A.* **2011**, *108* (4), 1228–1233.
- (7) Hirao, H.; Kumar, D.; Que, L., Jr.; Shaik, S. Two-State Reactivity in Alkane Hydroxylation by Non-Heme Iron–Oxo Complexes. *J. Am. Chem. Soc.* **2006**, *128* (26), 8590–8606.
- (8) Kumar, D.; Hirao, H.; Que, L., Jr.; Shaik, S. Theoretical Investigation of C–H Hydroxylation by (N4Py)FeIVO2+: An Oxidant More Powerful than P450? *J. Am. Chem. Soc.* **2005**, *127* (22), 8026–8027.
- (9) England, J.; Martinho, M.; Farquhar, E. R.; Frisch, J. R.; Bominaar, E. L.; Münck, E.; Que, L., Jr. A Synthetic High-Spin Oxoiron(IV) Complex: Generation, Spectroscopic Characterization, and Reactivity. *Angew. Chem.* **2009**, *121* (20), 3676–3680.
- (10) Lacy, D. C.; Gupta, R.; Stone, K. L.; Greaves, J.; Ziller, J. W.; Hendrich, M. P.; Borovik, A. S. Formation, Structure, and EPR Detection of a High Spin Fe<sup>IV</sup>–Oxo Species Derived from Either an Fe<sup>III</sup>–Oxo or Fe<sup>III</sup>–OH Complex. *J. Am. Chem. Soc.* **2010**, *132* (35), 12188–12190.
- (11) Bigi, J. P.; Harman, W. H.; Lassalle-Kaiser, B.; Robles, D. M.; Stich, T. A.; Yano, J.; Britt, R. D.; Chang, C. J. A High-Spin Iron(IV)–Oxo Complex Supported by a Trigonal Nonheme Pyrrolide Platform. *J. Am. Chem. Soc.* **2012**, *134* (3), 1536–1542.
- (12) Cho, K.-B.; Shaik, S.; Nam, W. Theoretical predictions of a highly reactive non-heme Fe(IV)=O complex with a high-spin ground state. *Chem. Commun.* **2010**, *46* (25), 4511–4513.
- (13) Panov, G. I.; Sobolev, V. I.; Dubkov, K. A.; Parmon, V. N.; Ovanesyan, N. S.; Shilov, A. E.; Shteinman, A. A. Iron complexes in zeolites as a new model of methane monooxygenase. *React. Kinet. Catal. Lett.* **1997**, *61* (2), 251–258.
- (14) Xiao, D. J.; Bloch, E. D.; Mason, J. A.; Queen, W. L.; Hudson, M. R.; Planas, N.; Borycz, J.; Dzubak, A. L.; Verma, P.; Lee, K.; et al. Oxidation of ethane to ethanol by N<sub>2</sub>O in a metal–organic framework with coordinatively unsaturated iron(II) sites. *Nat. Chem.* **2014**, *6*, 590–595.
- (15) Verma, P.; Vogiatzis, K. D.; Planas, N.; Borycz, J.; Xiao, D. J.; Long, J. R.; Gagliardi, L.; Truhlar, D. G. Mechanism of Oxidation of Ethane to Ethanol at Iron(IV)–Oxo Sites in Magnesium-Diluted Fe<sub>2</sub>(dobdc). *J. Am. Chem. Soc.* **2015**, *137* (17), 5770–5781.
- (16) Schröder, D.; Shaik, S.; Schwarz, H. Two-State Reactivity as a New Concept in Organometallic Chemistr. *Acc. Chem. Res.* **2000**, *33* (3), 139–145.
- (17) Biswas, A. N.; Puri, M.; Meier, K. K.; Oloo, W. N.; Rohde, G. T.; Bominaar, E. L.; Münck, E.; Que, L., Jr. Modeling TauD-J: A High-Spin Nonheme Oxoiron(IV) Complex with High Reactivity toward C–H Bonds. *J. Am. Chem. Soc.* **2015**, *137* (7), 2428–2431.
- (18) Kazaryan, A.; Baerends, E. J. Ligand Field Effects and the High Spin–High Reactivity Correlation in the H Abstraction by Non-Heme Iron(IV)–Oxo Complexes: A DFT Frontier Orbital Perspective. *ACS Catal.* **2015**, *5* (3), 1475–1488.
- (19) Hirao, H.; Ng, W. K. H.; Moeljadi, A. M. P.; Bureekaew, S. Multiscale Model for a Metal–Organic Framework: High-Spin Rebound Mechanism in the Reaction of the Oxoiron(IV) Species of Fe-MOF-74. *ACS Catal.* **2015**, *5* (6), 3287–3291.
- (20) Chung, Y. G.; Camp, J.; Haranczyk, M.; Sikora, B. J.; Bury, W.; Krungleviciute, V.; Yildirim, T.; Farha, O. K.; Sholl, D. S.; Snurr, R. Q. Computation-Ready, Experimental Metal–Organic Frameworks: A Tool To Enable High-Throughput Screening of Nanoporous Crystals. *Chem. Mater.* **2014**, *26* (21), 6185–6192.
- (21) Haldoupis, E.; Vogiatzis, K. D.; Gagliardi, L.; Siepmann, J. I. Computational Screening of Metal–Organic Frameworks with Open Metal Sites for Carbon Capture. Manuscript in preparation.
- (22) Jiang, B.; Liu, Z. Poly[[aqua(μ-4,4′-bipyridyl-κ<sup>2</sup>N:N′)bis(μ-formato-κ<sup>2</sup>O:O′)iron(II)] tetrahydrate]. *Acta Crystallogr., Sect. E: Struct. Rep. Online* **2009**, *65*, m1189–m1190.
- (23) Wang, X.-F.; Zhang, Y.-B.; Zhang, W.-X.; Xue, W.; Zhou, H.-L.; Chen, X.-M. Buffering additive effect in the formation of metal–carboxylate frameworks with slightly different linear M<sub>3</sub>(RCOO)<sub>6</sub> clusters. *CrystEngComm* **2011**, *13* (12), 4196–4201.
- (24) Liu, W.-T.; Li, J.-Y.; Ni, Z.-P.; Bao, X.; Ou, Y.-C.; Leng, J.-D.; Liu, J.-L.; Tong, M.-L. Incomplete Spin Crossover versus Antiferromagnetic Behavior Exhibited in Three-Dimensional Porous Fe(II)-Bis(tetrazolate) Frameworks. *Cryst. Growth Des.* **2012**, *12* (3), 1482–1488.
- (25) Wharmby, M. T.; Pearce, G. M.; Mowat, J. P. S.; Griffin, J. M.; Ashbrook, S. E.; Wright, P. A.; Schilling, L.-H.; Lieb, A.; Stock, N.; Chavan, S.; et al. Synthesis and crystal chemistry of the STA-12 family of metal N,N′-piperazinebis(methylenephosphonate)s and applications of STA-12(Ni) in the separation of gases. *Microporous Mesoporous Mater.* **2012**, *157*, 3–17.
- (26) Sumida, K.; Horike, S.; Kaye, S. S.; Herm, Z. R.; Queen, W. L.; Brown, C. M.; Grandjean, F.; Long, G. J.; Dailly, A.; Long, J. R. Hydrogen storage and carbon dioxide capture in an iron-based sodalite-type metal–organic framework (Fe-BTT) discovered via high-throughput methods. *Chem. Sci.* **2010**, *1* (2), 184–191.
- (27) Li, X.; Wu, B.-L.; Niu, C.-Y.; Niu, Y.-Y.; Zhang, H.-Y. Syntheses of Metal–2-(Pyridin-4-yl)-1H-imidazole-4,5-dicarboxylate Networks with Topological Diversity: Gas Adsorption, Thermal Stability and Fluorescent Emission Properties. *Cryst. Growth Des.* **2009**, *9* (8), 3423–3431.
- (28) Ma, S.; Yuan, D.; Chang, J.-S.; Zhou, H.-C. Investigation of Gas Adsorption Performances and H<sub>2</sub> Affinities of Porous Metal–Organic

Frameworks with Different Entatic Metal Centers. *Inorg. Chem.* **2009**, *48* (12), 5398–5402.

(29) Sumida, K.; Stück, D.; Mino, L.; Chai, J.-D.; Bloch, E. D.; Zavorotynska, O.; Murray, L. J.; Dincă, M.; Chavan, S.; Bordiga, S.; et al. Impact of Metal and Anion Substitutions on the Hydrogen Storage Properties of M-BTT Metal–Organic Frameworks. *J. Am. Chem. Soc.* **2013**, *135* (3), 1083–1091.

(30) Dincă, M.; Dailly, A.; Liu, Y.; Brown, C. M.; Neumann, D. A.; Long, J. R. Hydrogen Storage in a Microporous Metal–Organic Framework with Exposed Mn<sup>2+</sup> Coordination Sites. *J. Am. Chem. Soc.* **2006**, *128* (51), 16876–16883.

(31) Brozek, C. K.; Cozzolino, A. F.; Teat, S. J.; Chen, Y.-S.; Dincă, M. Quantification of Site-Specific Cation Exchange in Metal–Organic Frameworks Using Multi-Wavelength Anomalous X-ray Dispersion. *Chem. Mater.* **2013**, *25* (15), 2998–3002.

(32) Furukawa, H.; Müller, U.; Yaghi, O. M. Heterogeneity within Order” in Metal–Organic Frameworks. *Angew. Chem., Int. Ed.* **2015**, *54* (11), 3417–3430.

(33) Fang, Z.; Bueken, B.; De Vos, D. E.; Fischer, R. A. Defect-Engineered Metal–Organic Frameworks. *Angew. Chem., Int. Ed.* **2015**, *54* (25), 7234–7254.

(34) Sholl, D. S.; Lively, R. P. Defects in Metal–Organic Frameworks: Challenge or Opportunity? *J. Phys. Chem. Lett.* **2015**, *6* (17), 3437–3444.

(35) Ravon, U.; Savonnet, M.; Aguado, S.; Domine, M. E.; Janneau, E.; Farrusseng, D. Engineering of coordination polymers for shape selective alkylation of large aromatics and the role of defects. *Microporous Mesoporous Mater.* **2010**, *129* (3), 319–329.

(36) Dhakshinamoorthy, A.; Alvaro, M.; Horcajada, P.; Gibson, E.; Vishnuvarthan, M.; Vimont, A.; Grenèche, J.-M.; Serre, C.; Daturi, M.; Garcia, H. Comparison of Porous Iron Trimesates Basolite F300 and MIL-100(Fe) As Heterogeneous Catalysts for Lewis Acid and Oxidation Reactions: Roles of Structural Defects and Stability. *ACS Catal.* **2012**, *2* (10), 2060–2065.

(37) Ameloot, R.; Vermoortele, F.; Hofkens, J.; De Schryver, F. C.; De Vos, D. E.; Roeyfaers, M. B. J. Three-Dimensional Visualization of Defects Formed during the Synthesis of Metal–Organic Frameworks: A Fluorescence Microscopy Study. *Angew. Chem., Int. Ed.* **2013**, *52* (1), 401–405.

(38) Platero-Prats, A. E.; Mavrandonakis, A.; Gallington, L. C.; Liu, Y.; Hupp, J. T.; Farha, O. K.; Cramer, C. J.; Chapman, K. W. Structural Transitions of the Metal-Oxide Nodes within Metal–Organic Frameworks: On the Local Structures of NU-1000 and UiO-66. *J. Am. Chem. Soc.* **2016**, *138* (12), 4178–4185.

(39) Xiao, D. J.; Gonzalez, M. I.; Darago, L. E.; Vogiatzis, K. D.; Haldoupis, E.; Gagliardi, L.; Long, J. R. Selective, Tunable O<sub>2</sub> Binding in Cobalt(II)–Triazolate/Pyrazolate Metal–Organic Frameworks. *J. Am. Chem. Soc.* **2016**, *138*, 7161.

(40) Reed, D. A.; Xiao, D. J.; Gonzalez, M. I.; Darago, L. E.; Herm, Z. R.; Grandjean, F.; Long, J. R. Reversible CO Scavenging via Adsorbate-Dependent Spin State Transitions in an Iron(II)–Triazolate Metal–Organic Framework. *J. Am. Chem. Soc.* **2016**, *138* (17), 5594–5602.

(41) Wilmer, C. E.; Leaf, M.; Lee, C. Y.; Farha, O. K.; Hauser, B. G.; Hupp, J. T.; Snurr, R. Q. Large-scale screening of hypothetical metal–organic frameworks. *Nat. Chem.* **2012**, *4*, 83–89.